Magnetization-based assessment of correlation energy in canted single-chain magnets

A. Barasiński,[1] G. Kamieniarz,[2] and A. Drzewiński[1]

[1]*Institute of Physics, University of Zielona Góra, ul. Prof. Z. Szafrana 4a, 65-516 Zielona Góra, Poland*
[2]*A. Mickiewicz University, Faculty of Physics, ul. Umultowska 85, 61-614 Poznań, Poland*

We demonstrate numerically that for the strongly anisotropic homometallic $S = 2$ canted single-chain magnet described by the quantum antiferromagnetic Heisenberg model, the correlation energy and exchange coupling constant can be directly estimated from the in-field-magnetization profile found along the properly selected crystallographic direction. In the parameter space defined by the spherical angles (ϕ, θ) determining the axes orientation, four regions are identified with different sequences of the characteristic field-dependent magnetization profiles representing the antiferromagnetic, metamagnetic, and weak ferromagnetic type behavior. These sequences provide a criterion for the applicability of the anisotropic quantum Heisenberg model to a given experimental system. Our analysis shows that the correlation energy decreases linearly with field and vanishes for a given value H_{cr}, which defines a special coordinates in the metamagnetic profile relevant for the zero-field correlation energy and magnetic coupling. For the single-chain magnet formed by the strongly anisotropic manganese(III) acetate meso-tetraphenylporphyrin complexes coupled to the phenylphosphinate ligands, the experimental metamagnetic-type magnetization curve in the c direction yields an accurate estimate of the values of correlation energy $\Delta_\xi/k_B = 7.93$ K and exchange coupling $J/k_B = 1.20$ K.

I. INTRODUCTION

Molecular magnets make a wide emerging class of new materials whose properties extend the range of those typically associated with magnets, i.e., they offer low density, transparency, electrical insulation, and a possibility of low-temperature synthesis.[1] Single-chain magnets (SCM) belonging to the class of molecular magnets have been of particular interest since Gatteschi *et al.*[2] discovered slow relaxation of magnetization in a chain compound, comprising Co(II) centers, and organic radicals, without any evidence of phase transition to a three-dimensional magnetic ordering. Soon after, Clerac *et al.* discovered similar magnetic properties in an $S = 3$ Heisenberg ferromagnetic chain comprising Mn(III)-Ni(II)-Mn(III) trimers with an easy axis parallel to the chain.[3] Next, other SCM systems often based on ferrimagnetic chains containing alternating spins of unequal magnitude were discovered.[4] The slow magnetic relaxation arises from large uniaxial magnetic anisotropy, negligible magnetic interactions between the chains, and considerable intrachain interactions.[1,5] The last condition is desirable for raising the blocking temperature. Moreover, for some one-dimensional quantum spin systems with competing nearest-neighbor and next-nearest-neighbor interactions,[6] the single-chain magnetic behavior can be affected with frustration.[7]

The simplest description of ferromagnetic SCMs is based on the Glauber theory if the limit of an Ising chain can be explored.[8] The Ising ferromagnetic chains display slow relaxation of magnetization and the relaxation time τ depends on the spin-pair correlations. For these chains, the correlation length ξ diverges exponentially at low temperatures as

$$\xi = C_0 \exp(\Delta_\xi/k_B T), \qquad (1)$$

where Δ_ξ is the correlation energy and k_B is the Boltzmann constant.[9] The exponent Δ_ξ is proportional to the activation energy, which enters the Arrhenius law[9] and can be directly estimated from the experimental static susceptibility of the chain by the relation $\xi \sim \chi T$, plotting $\ln(\chi T)$ as a function of $1/T$. The correlation energy is also referred to as the energy to create a domain wall. Important fact is that Δ_ξ is proportional to the magnetic coupling constant[9] and similar conclusions remain valid for the antiferromagnetic Ising model[5,10] but then $\xi \sim 1/(\chi T)$. In addition, the correlation energy Δ_ξ is also the main part of the additive term determining the relaxation time in the Ising-like and anisotropic classical Heisenberg chains.[9,11]

The relations between the correlation length and the zero-field susceptibility as well as between the correlation energy and the magnetic coupling can be used for the classical ferromagnetic Heisenberg model in the strong anisotropy limit.[9,12,13] If the Hamiltonian is defined by

$$\mathcal{H} = J \sum_{i=1}^{L-1} \left(S_i^x S_{i+1}^x + S_i^y S_{i+1}^y + S_i^z S_{i+1}^z \right) + D \sum_{i=1}^{L} S_i^z S_i^z,$$

the limit is reached when the exchange coupling J and the single-ion anisotropy D satisfy the relation $|D/J| > 2/3$. Then the correlation energy calculated from the product χT yields the value of the coupling J because[9]

$$\Delta_\xi = 2|J|S^2.$$

For ferromagnetic systems, this scenario is well confirmed[9,14,15] and has been exploited for a number of compounds,[16,17] but for antiferromagnetic chains with non-collinear anisotropy axes[11,18] the situation is much less clear. The problem was revealed[11] for the compound of formula [Mn(TPP)O$_2$PHPh]·H$_2$O considered a textbook example of SCM (TPP = *meso*-tetraphenylporphyrin and PHPh = phenylphosphinate) and referred to as Mn-CAF (canted antiferromagnet). It was possible to rationalise many experimental results performed on Mn-CAF, assuming the generalized expression for the correlation energy in

the form

$$\Delta_\xi = 2|J|S^2 \cos \delta, \tag{2}$$

where δ is the canting angle for two classical spins oriented along the anisotropy axes. However, the proportionality between the correlation length ξ and the product χT was ruled out, implying that the correlation energy cannot be determined by the magnetic measurement of the static susceptibility.

In this paper, we demonstrate that the correlation energy of the quantum model of a canted antiferromagnetic chain can be found from the in-field single-crystal magnetization profile properly chosen and its δ dependence is given by the classical expression (2). These results suggest that the correlation energy Δ_ξ can be estimated from the in-field magnetization measurements. As soon as the spin value, the geometrical structure and Δ_ξ are known, the value J of the magnetic coupling follows from Eq. (2). Considering the empirical shape of the magnetization isotherm in the c direction for Mn-CAF, we directly find the J value without any fitting procedure.

The paper is organized as follows: Sec. II is devoted to a model describing the anisotropic quantum spin systems and the numerical method for accurate calculations of magnetic properties in a wide temperature range. Section III is dedicated to presentation of results and their discussion. Section IV concludes our paper, summarizing the main outcomes.

II. MODEL AND DMRG METHOD FOR CANTED SINGLE-CHAIN MAGNETS

We consider the quantum anisotropic Heisenberg model, which is needed to get quantitative estimates of the thermodynamic properties[19,20] of the chains with noncollinear anisotropy axes:

$$\mathcal{H} = J \sum_{i=1}^{L-1} \left(S_i^a S_{i+1}^a + S_i^b S_{i+1}^b + S_i^c S_{i+1}^c \right)$$
$$+ \sum_{i=1}^{L} \sum_{\alpha\beta} \left(S_i^\alpha \hat{D}_i^{\alpha\beta} S_i^\beta + \mu_B H^\alpha \hat{g}_i^{\alpha\beta} S_i^\beta \right), \tag{3}$$

where spin $S = 2$ and L stands for the length of the chain. The exchange coupling J between nearest-neighbor spins is isotropic, uniform, and positive. The tensors representing the single-ion anisotropy $\hat{D}_i$ and $\hat{g}_i$ factors are nondiagonal and depend on angles (ϕ, θ) or $(-\phi, \theta)$ for odd and even sites, respectively. The indices $\alpha, \beta \in \{a,b,c\}$ define the global coordination system. The c direction is chosen along the chain axis and plays also the role of the quantization axis.

The explicit form of the tensors in the model (3) depends on the angles (ϕ, θ) defining the anisotropy axes (see Fig. 1) and is given in the previous publications.[11,19] We note that for all the pairs of angles (ϕ, θ) the canting angle is determined from the relation

$$\cos \delta = \sin^2(\theta) \cos(2\phi) + \cos^2(\theta).$$

Analysis of our model (3) is based on the numerical quantum transfer matrix method,[20–24] where the partition function of the quantum chain is mapped onto the partition function of the classical $2d$ system with multispin interactions
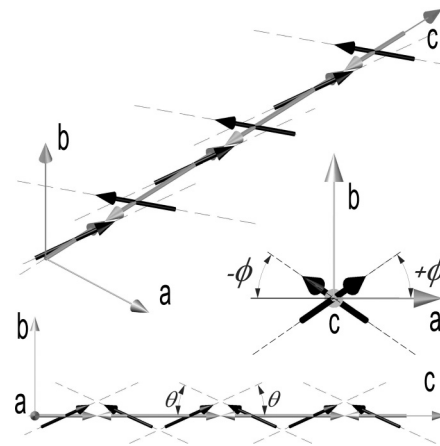

FIG. 1. Schematic views of the chain structure in the global coordination system $\{a,b,c\}$, where the spherical angles (ϕ, θ) are defined. The black arrows represent the canted Mn-CAF spin arrangement, whereas the gray ones correspond to the collinear antiferromagnetic spin arrangement ($\phi = 0$, $\theta = 0$).

and a finite width $2M$.[25,26] For different values of M, called the Trotter number, the classical partition functions form a series of approximants Z_M, where the leading errors are of the order of $1/M^2$. The higher the value of M, the better the quantum nature of the problem is taken into account. As the Hilbert space dimension increases exponentially with increasing Trotter number, computations are feasible only for relatively small M. To overcome this problem, we employ the density-matrix renormalization group technique (DMRG)[27–31] for determining an effective Hamiltonian representation in the Hilbert subspace of a given size m that ensures covering the entire experimental temperature range.

The DMRG method is very powerful but it is computationally demanding as far as the resources and programming are concerned. The transfer matrices are asymmetric and the corresponding density matrices, constructed from the right and left eigenvectors of the largest eigenvalue $\lambda_{\max}$ of a transfer matrix, are non Hermitian. We were able to overcome these problems by applying complex algebra,[32] which guaranties the biorthogonality of complex eigenvectors but increases the computational complexity.

In some DMRG applications,[27] the Hilbert space is split into subspaces of fixed values of $M_{\text{stag}} = \sum (-1)^j S_j$, where S_j denotes a spin variable in a given column. Then the highest eigenvalue $\lambda_{\max}$ can be found in the block with the staggered magnetization $M_{\text{stag}} = 0$. This simplification follows from some symmetries which may occur in the four-spin DMRG vertices. For the noncollinear model this is not the case, therefore $\lambda_{\max}$ has to be found in the entire Hilbert space.

For each temperature, the free energy of the macroscopic system (3) per site ($L \to \infty$) is related to the maximum eigenvalue $\lambda_{\max}$ of the transfer matrix $\mathcal{T}_M$,[33] whereas the magnetization and magnetic susceptibility can be obtained by taking the first and second derivatives of the free energy with respect to external magnetic field. These quantities are calculated in the subspace $0 \leqslant \phi \leqslant \pi/2$ and $0 \leqslant \theta \leqslant \pi/2$, which follows from the Hamiltonian symmetry.

The correlation length of the α components of spin is given by the following ratio[34]:

$$1/\xi_\alpha = -\lim_{R\to\infty} \frac{1}{R} \ln \langle S_i^\alpha S_{i+R}^\alpha \rangle$$

$$= -\lim_{M\to\infty} \lim_{R\to\infty} \lim_{L\to\infty} \frac{1}{R} \ln \frac{\mathrm{Tr}\, \mathcal{T}_M^i S^\alpha \mathcal{T}_M^R S^\alpha \mathcal{T}_M^{L-(i+R)}}{\mathrm{Tr}\, \mathcal{T}_M^L}$$

$$= \lim_{M\to\infty} \ln \frac{\lambda_{\max}}{\lambda_\nu}, \qquad (4)$$

where S^α is the tensor product of the α component of the spin operator and $2M-1$ identity matrices of $2S+1$ size. The $|\psi_{\max}\rangle$ vector corresponds to the $\lambda_{\max}$ eigenvalue, whereas the eigenvalue λ_ν is the highest among all whose eigenvector $|\psi_\nu\rangle$ that satisfy the condition $|\langle\psi_{\max}|S^\alpha|\psi_\nu\rangle| \neq 0$.

The convergence of the approximants with respect to M depends on temperature and the size of the optimal basis set m. Our results are provided for $m = 125$ and the Trotter number M up to 20 (the lower temperature the higher M is needed). According to our estimation, the accuracy of results in the whole parameter space considered is not lower than 0.5%.[20]

III. RESULTS AND DISCUSSIONS

Recently, several compounds of antiferromagnetic one-dimensional systems containing Mn(III) ions have been reported.[11,18] Here, the most interesting example[11] is Mn-CAF, where the anisotropy axes are defined by Jahn-Teller elongation of Mn(III) octahedra and make the angle $\theta = 21.01°$ with the chain direction parallel to the c axis (see Fig. 1). Projections of the anisotropy axes onto the plane perpendicular to the chain, alternate along the a crystallographic axis making angles $\phi = 56.55°$.

The single-crystal magnetometry measurements[11] revealed three patterns of the in-field-magnetization profiles. For the a direction, the pattern shows linear field dependence and is referred to as antiferromagnetic (AF). The field dependencies measured along the b and c are referred to as the weak ferro-magnetic (WF) and the metamagnetic type (MM), respectively.

Taking into account the known values of ϕ and θ angles and performing the Monte Carlo simulations, the values of exchange coupling, uniaxial anisotropy, and g factor were obtained (in short the Mn-CAF parameters) for the classical counterpart of the model (3),

$$J/k_B = 1.36(8)\,K, \quad D/k_B = -4.7(2)\,K, \quad g = 1.97(1),$$
$$(5)$$

fitting the experimental susceptibility and magnetization curves.[11] So, the high value of the ratio $|D/J| \simeq 3.5$ corresponding to a strong anisotropy occurred.

Using the classical Mn-CAF parameters (5) and the corresponding angles

$$\phi = 56.55°, \; \theta = 21.01°, \; \delta = 34.6°,$$

we have determined the in-field magnetization profiles for three crystallographic directions. Their features agree qualitatively with those published previously in Fig. 5 for Mn-CAF,[11] including the sequence of patterns AF, WF, and MM for the a, b, c directions. The MM-type profile for the field along the c axis was calculated earlier within DMRG[19,35] and its
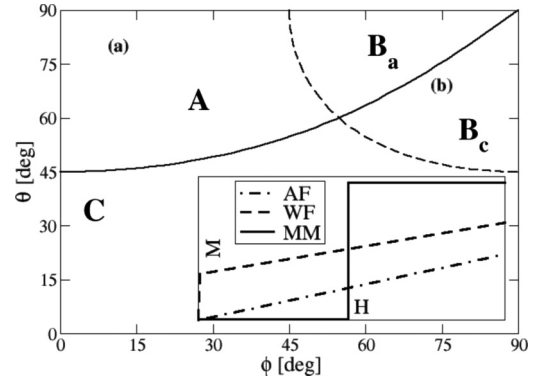

FIG. 2. The angle-dependent diagram showing sectors with different sequences of the in-field magnetization patterns. In sectors A, B, and C, the MM-type patterns occur in the a, b, c directions, respectively. All the patterns are outlined in the inset in the zero-temperature limit.

behavior detected some quantitative deviations with respect to the classical counterpart.

Relaxing the angles ϕ and θ, we have noticed that the sequence of the magnetization patterns varies with the easy axes orientation and we have established the domains (see Fig. 2) in the (ϕ, θ) parameter space. Within a given domain, the fixed shape of the low-temperature magnetization isotherms as a function of field for all the crystallographic directions occurs. The expected zero-temperature patterns are plotted in the inset. The sectors appearing in the diagram are described in Table I. In sectors A, B, and C, the MM-type patterns are unveiled for the field along the a, b, c axes, respectively. The sequence of the AF and WF profiles accompanying the MM-type shape in a given sector is specified in Table I. In the B sectors, the AF pattern is missing and two WF patterns are present in return. The crystallographic direction, where the magnetization values are higher in the low fields, has been distinguished by an additional index a (or b).

The B sectors in the diagram are separated from the other sectors by the dashed line obtained from the solution of the equation $\cot(2\theta) = \sin(2\phi)\cos(2\phi)$. This line corresponds to the canted angle between the adjacent anisotropy axes which amounts to $\delta = \pi/2$. The solid line in the diagram follows from the symmetry of the Hamiltonian and can be determined from the solution of the equation $\cot\theta = \cos\phi$.

The diagram in Fig. 2 provides the criterion whether the model (3) can describe a particular magnetic system. It predicts the occurrence of the MM-type profile, which is accompanied by a given combination of the AF-type and the WF-type patterns. We immediately see that the criterion is fulfilled

TABLE I. Pattern sequences in the diagram sectors.

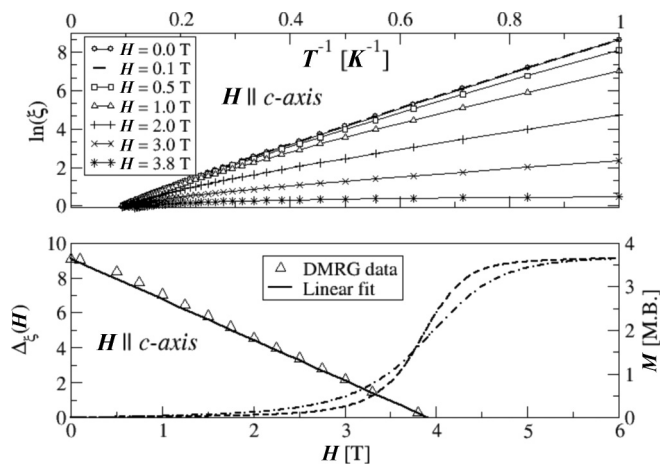| Sector symbol	Crystallographic direction		
	a	b	c
A	MM	WF	AF
B_a	WF	MM	WF
B_c	WF	MM	WF
C	AF	WF	MM

FIG. 3. (Top) Temperature behavior of the correlation length for various values of the magnetic field H parallel to the MM axis (the Mn-CAF parameters). (Bottom) Our estimations of the $\Delta_\xi(H)$ vs external magnetic field parallel to the c axis plotted by triangles. The solid line represents the linear regression $f(H) = 9.10 - 2.33H$. The magnetization isotherms at $T = 1$ and 1.6 K are given by the dashed and chain lines, respectively.

for Mn-CAF.[11] Its geometric coordinates (ϕ, θ) belong to the sector C and the experimental single-crystal profiles agree with the patterns predicted for this sector.

As the zero-field susceptibility and the correlation energy are not related for the canted antiferromagnetic chains, we have decided to analyze the field dependence of the correlation energy $\Delta_\xi(H)$. First, we checked if the correlation length diverges in the limit of low temperatures. For low temperatures, the upper panel of Fig. 3 demonstrates a linear dependence of $\ln(\xi_c)$ [where ξ_c is determined from Eq. (4)] on the inverse of temperature, choosing the Mn-CAF parameters (5) and the corresponding angles $\phi = 56.55°$ and $\theta = 21.01°$. This dependence implies that the low-temperature correlation length ξ exhibits the exponential divergence in the MM direction,

$$\xi = C_0 \exp[\Delta_\xi(H)/k_B T], \tag{6}$$

but the slope $\Delta_\xi(H)$ is field dependent.

The field dependence of the correlation energy $\Delta_\xi(H)$ has been studied numerically and plotted by triangles in the bottom part of Fig. 3. We have revealed a striking linear behavior, which can be very well reproduced by the function

$$\Delta_\xi(H)/k_B = 9.10 - 2.33H, \tag{7}$$

where the right-hand side is expressed in kelvin and the field is given in tesla. So, the function $\Delta_\xi(H)$ vanishes, which implies a finite value of correlation length ξ [see Eq. (6)], for the critical field $H_{cr} = 3.91$ T, which is close to the value estimated directly from the DMRG correlation length, $H_{cr} = 3.86$ T.

The abrupt change of the correlation length from the infinite to the finite value induced by the field should be accompanied by some changes in the physical properties. We demonstrate in the bottom panel of Fig. 3 that the MM-type profile displays a rapid jump in the vicinity of H_{cr} from 0 to a nearly saturation value. We interpret this behavior as a field-driven transition from the antiferromagnetic to the ferromagnetic order along the c direction. Such critical field can be determined from the
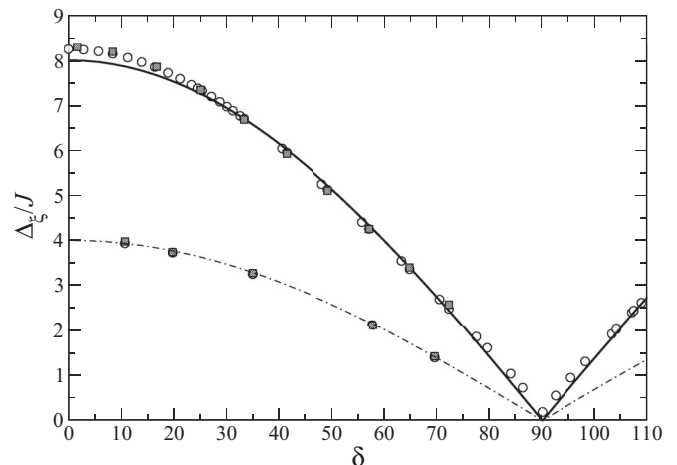

FIG. 4. Comparison between the functions $2S^2|\cos(\delta)|$ and $S^2|\cos(\delta)|$ vs δ plotted by the full and the dashed line, respectively, and the ratios Δ_ξ/J and $\mu_B M_{cr} H_{cr}/J$ illustrated by the circles and squares. The open symbols correspond to $J/k_B = 1.26$ K and the full symbols to $J/k_B = 1.36$ K.

intersection of the low-temperature magnetization isotherms, from their inflection point or from the maximum of the in-field magnetic susceptibility.

Now we analyze the correlation energy Δ_ξ for the Mn-CAF parameters in the absence of a magnetic field. Equation (7) implies $\Delta_\xi(H = 0)/k_B = 9.10$ K, while the DMRG calculations based on Eqs. (1) and (4) yield $\Delta_\xi/k_B = 9.05$ K. These estimates are in remarkable agreement with the classical prediction[11] $\Delta_\xi = 8.95$ K following from Eq. (2). Moreover, the coincidence of the correlation energy of the quantum model (3) and the classical dependence (2) is confirmed and demonstrated for a number of couplings J and the canting angles δ in Fig. 4.

In Fig. 4, the upper continuous and lower dashed lines represent the functions $2S^2 \cos\delta$ and $S^2 \cos\delta$, respectively. The open and full circles illustrate the ratios Δ_ξ/J calculated numerically within DMRG for $J/k_B = 1.26$ and 1.36 K, respectively. As to the angles δ, their values follow from the angles ϕ and θ chosen from different sectors of the diagram in Fig. 2. The fields were applied in the proper direction for a sector selected.

We conclude that the agreement between the classical predictions $2S^2 \cos\delta$ for the ratio Δ_ξ/J and those calculated for our quantum model (3) and plotted in Fig. 4 is very good. There are some deviation for small and high values of δ, but they can be attributed to uncertainties of the extrapolations performed for $\ln(\xi)$ yielding the values Δ_ξ. These uncertainties are of the order of a few percent and are much higher than the accuracy of the DMRG results. They could be diminished lowering temperature and increasing the cost of our simulations. Concluding, our numerical results in Fig. 4 give a strong evidence that the correlation energy of the canted antiferromagnetic quantum chains can be expressed by Eq. (2) previously found for the classical systems.

In Fig. 4, we also plot by the full squares the ratios $\mu_B M_{cr} H_{cr}/J$ as a function of δ, where M_{cr} is the value of the MM-type magnetization profile corresponding to the field

H_{cr}. We emphasise that the ratio is completely determined by the coordinates of the inflection point of the MM-type magnetization profile. The ratios $\mu_B M_{\mathrm{cr}} H_{\mathrm{cr}}/J$ calculated coincide with the values of the function $S^2 \cos \delta$ drawn by the dashed line and are lower by a factor of 2 than the ratios Δ_ξ/J, implying that

$$\Delta_\xi = 2\mu_B M_{\mathrm{cr}} H_{\mathrm{cr}}. \tag{8}$$

We can interpret the result (8) that the correlation energy is equal to the average Zeeman energy per pair of spins calculated for the critical field H_{cr}.

The relation (8) is an important result of our paper because it provides a direct estimate of the correlation energy Δ_ξ in terms of the special coordinates of the MM-type magnetization profile. Moreover, the exchange constant J/k_B can be also obtained from the MM-type single-crystal low-temperature magnetization isotherm. Combining Eqs. (2) and (8), we find the formula for the magnetic coupling:

$$J = \mu_B M_{\mathrm{cr}} H_{\mathrm{cr}}/(S^2 \cos \delta). \tag{9}$$

To validate our conclusions, in Fig. 5 the MM-type behavior is drawn for the ratios $|D/J| \simeq 3.5$ and 4.5 in both panels. For the angles specified in the legends and coming from the sectors A and B, the (a) and (b) panels display the profiles found for the magnetic field parallel to the a and b axes, respectively. The slope of all the MM-type curves in Fig. 5 increases with decreasing temperature and the shape does not change.

The coordinates of the intersections of the corresponding magnetization isotherms in Fig. 5 ($T = 1.0$ and 1.6 K) inserted into Eq. (9) yield the consistent estimates of J/k_B with the uncertainty equal to ± 0.04 K for the input values $J/k_B = 1.26$ and 1.36 K. When we used lower temperatures ($T = 0.5$ and 1.0 K), the uncertainty declined to ± 0.005 K for the same J/k_B, which is the expected trend.

Now, taking the values $\delta = 34.6°$, $H_{\mathrm{cr}} = 3.45$ T, and $M_{\mathrm{cr}} = 1.71$ (in μ_B) directly from the experiment for Mn-CAF compound,[11] we can evaluate from Eqs. (8) and (9) the value of correlation energy $\Delta_\xi/k_B = 7.93$ K and the coupling constant $J/k_B = 1.20$ K, respectively. Both the values are slightly lower than the $\Delta_\xi/k_B = 8.95$ K and $J/k_B = 1.36(8)$ K reported earlier.[11] However, this fact can be understood as the experimental value $J/k_B = 1.36(8)$ K was settled on the basis of the classical model and the fitting procedure which usually overestimate the coupling constant.[20] If the coupling J is overestimated then the relation (2) may proliferate the inaccuracy and imply somewhat higher Δ_ξ.

IV. CONCLUSIONS

Our investigation has confirmed that the relative positions of the anisotropy axes affect the shape of magnetization curves along different crystallographic directions. The resulting angle-dependent diagram predicts four areas, each characterized by a specific sequence of the in-field magnetization patterns. If for a compound studied the shapes of magnetization curves in the low-temperature range are consistent with those established in the diagram for a given geometry, then the compound can be analyzed in terms of the quantum Heisenberg model with a strong anisotropy.

For the canted antiferromagnet SCM, the values of correlation energy $\Delta_\xi(H)$ decrease linearly with the applied field and vanish at H_{cr}, which coincides with the intersection point of the MM-type magnetization profiles. The coordinates H_{cr} and M_{cr} of this special point determine the zero-field correlation energy Δ_ξ, which in turn reveals the classical dependence on the canting angle δ and the coupling J. These findings relate the J value to the coordinates H_{cr} and M_{cr} and yield a simple recipe to the evaluation of J. Following these ideas, we have estimated for the Mn-CAF compound the relevant quantities at $\Delta_\xi/k_B = 7.93$ K and $J/k_B = 1.20$ K, which agree very well with the values reported earlier.

Our calculations provide some insight into the common claim that in the strong anisotropy limit the Heisenberg model can be substituted by the Ising model. We confirm that the projections of spins onto the axis displaying the MM-type pattern can be treated as classical Ising-type variables. Then the rapid jump in the magnetization profile can be related to formation of an Ising domain wall. Anyway, it is striking that the quantity Δ_ξ defined in the absence of field can be so easily settled from the experiment performed in the presence of field.
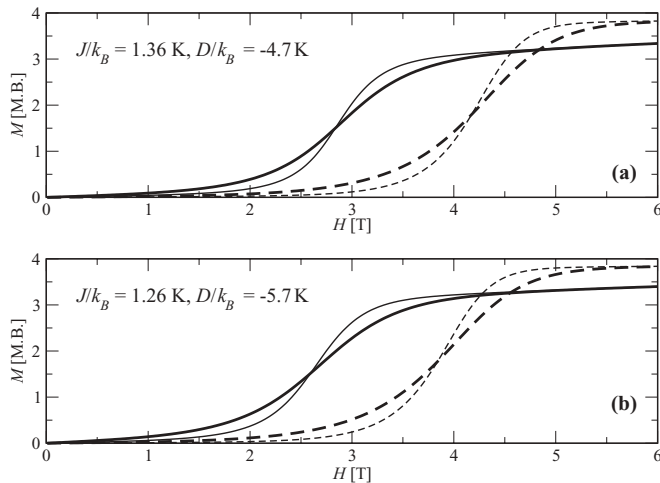

FIG. 5. Metamagnetic profiles as a function of magnetic field for two sets of parameters presented in the legends. The thick lines correspond to $T = 1.6$ K and the thin lines to $T = 1.0$ K. The solid and the dashed lines belong to the A sector ($\phi = 10°$, $\theta = 80°$) and to the B_C sector ($\phi = 75°$, $\theta = 65°$), respectively.

[1] Dante Gatteschi, Roberta Sessoli, and Jacques Villain, *Molecular Nanomagnets* (Oxford University Press, Oxford, 2006).

[2] A. Caneschi, D. Gatteschi, N. Lalioti, C. Sangregorio, R. Sessoli, G. Venturi, A. Vindigni, A. Rettori, M. G. Pini, and M. A. Novak, Angew. Chem. Int. Ed. **40**, 1760 (2001).

[3] R. Clerac, H. Miyasaka, M. Yamashita, and C. Coulon, J. Am. Chem. Soc. **124**, 12837 (2002).

[4] H. Miyasaka, T. Madanbashi, K. Sugimoto, Y. Nakazawa, W. Wernsdorfer, K. Sugiura, M. Yamashita, C. Coulon, and R. Clerac, Chem. Eur. J. **12**, 7028 (2006).

[5] C. Coulon, H. Miyasaka, and R. Cleérac, Struct. Bond. **122**, 163 (2006); H. Miyasaka and M. Yamashita, Dalton Trans. 2007, 399 (2007) , and references therein.

[6] N. B. Ivanov, J. Richter, and U. Schollwock, Phys. Rev. B **58**, 14456 (2007).

[7] Y.-Z. Zheng, W. Xue, W.-X. Zhang, M.-L. Tong, X.-M. Chen, F. Grandjean, G. J. Long, S.-W. Ng, P. Panissod, and M. Drillon, Inorg. Chem. **48**, 2028 (2009).

[8] R. J. Glauber, J. Math. Phys. **4**, 294 (1963).

[9] H. Miyasaka, M. Julve, M. Yamashita, and R. Clerac, Inorg. Chem. **48**, 3420 (2009).

[10] M. G. Pini and A. Rettori, Phys. Rev. B **76**, 064407 (2007).

[11] K. Bernot, J. Luzon, R. Sessoli, A. Vindigni, J. Thion, S. Richeter, D. Leclercq, J. Larionova, and A. van der Lee, J. Am. Chem. Soc. **130**, 1619 (2008).

[12] B. Barbara, J. Phys. **34**, 1039 (1973).

[13] J. M. Loveluck, S. W. Lovesey, and S. J. Aubry, Phys. C: Solid State Phys. **8**, 3841 (1975).

[14] C. Coulon, R. Clerac, L. Lecren, W. Wernsdorfer, and H. Miyasaka, Phys. Rev. B **69**, 132408 (2004).

[15] A. Saitoh, H. Miyasaka, M. Yamashita, and R. Clerac, J. Mater. Chem. **17**, 2002 (2007).

[16] J. Boeckmann, M. Wriedt, and C. Näther, Chem. Eur. J. **18**, 5284 (2012).

[17] Y-Z. Zheng, W. Xue, M-L. Tong, X-M. Chen, F. Grandjean, and G. J. Long, Inorg. Chem. **47**, 4077 (2008).

[18] Jung Hee Yoon, Dae Won Ryu, Hyoung Chan Kim, Sung Won Yoon, Byoung Jin Suh, and Chang Seop Hong, Chem. Eur. J. **15**, 3661 (2009).

[19] A. Barasiński, G. Kamieniarz, and A. Drzewiński, Comp. Phys. Comm. **182**, 2013 (2011).

[20] P. Sobczak, A. Barasiński, G. Kamieniarz, and A. Drzewiński, Phys. Rev. B **84**, 224431 (2011).

[21] G. Kamieniarz, R. Matysiak, A. C. D'Auria, F. Esposito, and U. Esposito, Phys. Rev. B **56**, 645 (1997).

[22] A. Caramico D'Auria, F. Esposito, U. Esposito, D. Gatteschi, G. Kamieniarz, and S. Wałcerz, J. Chem. Phys. **109**, 1613 (1998).

[23] G. Kamieniarz, M. Bieliński, and J.-P. Renard, Phys. Rev. B **60**, 14521 (1999).

[24] R. Matysiak, G. Kamieniarz, P. Gegenwart, and A. Ochiai, Phys. Rev. B **79**, 224413 (2009).

[25] M. Suzuki, Prog. Theor. Phys. **56**, 1454 (1976).

[26] T. Delica and H. Leschke, Physica A **176**, 736 (1990).

[27] X. Q. Wang and T. Xiang, Phys. Rev. B **56**, 5061 (1997).

[28] U. Schollwoeck, Rev. Mod. Phys. **77**, 259 (2005); K. Hallberg, Adv. Phys. **55**, 477 (2006); U. Schollwoeck, Ann. Phys. (NY) **326**, 96 (2011).

[29] A. Maciołek, A. Drzewiński, and R. Evans, Phys. Rev. B **64**, 056137 (2001).

[30] A. Drzewiński, A. Maciołek, A. Barasiński, and S. Dietrich, Phys. Rev. E **79**, 041145 (2009).

[31] N. Shibata, J. Phys. A: Math. Gen. **36**, R381 (2003).

[32] A. Barasiński, P. Sobczak, A. Drzewiński, G. Kamieniarz, A. Bieńko, J. Mroziński, and D. Gatteschi, Polyhedron **29**, 1485 (2010).

[33] R. J. Baxter, *Exactly Solved Models in Statistical Mechanics* (Academic Press, London, 1982).

[34] N. Hatano and M. Suzuki, J. Phys. Soc. J. **62**, 1346 (1993).

[35] G. Kamieniarz, P. Kozlowski, M. Antkowiak, P. Sobczak, T. Ślusarski, D. M. Tomecka, A. Barasiński, B. Brzostowski, A. Drzewiński, A. Bieńko, J. Mroziński, Acta Phys. Pol. A. **121**, 992 (2012).